The International Journal of Advanced Manufacturing Technology (2019) 101:2205–2216
https://doi.org/10.1007/s00170-018-3120-5

ORIGINAL ARTICLE

Machined channel quality and tool life using cermet micro-mill in micro-milling aluminum alloy

ShaSha Li [1,2,3] · Bin Zou [1,2] · Kaitao Xu [1,2] · YishunWang [1,2]

Received: 28 September 2018 / Accepted: 20 November 2018 / Published online: 28 November 2018

Abstract
Based on the superiority of self-developed cermet micro-mill over commercial cemented tungsten micro-mill in our previous work, the cutting characteristics, machined channel quality, and tool wear were investigated in this work, aiming at the evaluation of tool performance of this cermet micro-mill during micro-milling aluminum alloy 2024. Burrs and dimensional accuracy of machined channels, tool wear, and chip morphology were analyzed at various cutting parameters. The machining and forming mechanism related with cermet micro-mill were thoroughly discussed. It indicated that the cutting conditions can be optimized to enhance the performance of cermet micro-mills. The optimum cutting parameter can produce not only the good quality and high dimensional accuracy of channel with few small burrs but also the tool wear to a small degree ever after micro-milling of 10–20 min. The cermet micro-mill also exhibited the good capacity to break the chip. The good performance of cermet micro-mill was attributed to its good chemical stability and high hardness, especially the gained sharper tool tips and edges, and their better stability.

Keywords Aluminum alloys · Ceramic · Micro-mill · Tool wear · Micro-channels

1 Introduction

At present, many microproducts and components with complex features are applied in various industries, such as aerospace, electronics, medicine and biotechnology. To manufacture these components efficiently and precisely, various manufacturing processes, such as laser machining, electromechanical machining and electro-discharge machining, have been developed in recent years [1, 2]. However micro machining using miniature cutting tools has recently gained increasing interests because it has some virtues of better stiffness, higher productivity and lower cost [3]. Micro milling is one of the most important micro machining processes. Micro milling is kinematically similar to conventional milling process because it is a downscaled process of conventional milling, however micro milling and conventional milling have significant differences. The micro milling tool is the uppermost factor determining the micro milling process that requires tool materials with high strength and hardness in order to avoid fracture failures. The limitations of manufacturing technology make the fabrication of micro-milling tool be a difficult task. Moreover, the micro milling breaks easily during machining owing to its small diameter. At present, poly-crystalline (PCD) and cemented tungsten (WC) are widely used as tool materials to develop the micro-mills. Zhan et al. [4] used the wire EDM method to fabricate PCD micro-mill for precision milling of cemented tungsten. Suzuki et al. [5] also manufactured the micro-cutting tool with single crystalline diamond to make the holes and slots of 3 μm depth on ceramic. However, PCD micro-cutting tools are not able to meet the demands of machining ferrous metals [6]. The higher chemical affinity of PCD with ferrous metals leads to a rapid reduction of tool performance in machining. Compared to PCD micro mill, WC micro-mill has not only the better mechanical properties avoiding being broken but also the higher electrical conductivity allowing to be manufactured by EDM [7]. Egashira et al.

✉ Bin Zou
zou20011110@163.com

[1] Center for Advanced Jet Engineering Technologies (CaJET), School of Mechanical Engineering, Shandong University, 17923 Jing Shi Road, Jinan 250061, People's Republic of China

[2] Key Laboratory of High Efficiency and Clean Mechanical Manufacture, Ministry of Education, Shandong University, Shandong, China

[3] Shandong Special Equipment Inspection Institute Co., Ltd., Shandong, China

[8] developed a WC micro-mill with a diameter of 3 μm to conduct a micro-slot by a micro-milling process. A design criteria of micro-mills was put forward by Aurich et al. [9], that is, the single-edge shape is suitable for micro-mill with a diameter between 10 and 50 μm, and a micro-mill with a variable helix angle is suitable for the diameter ranging from 50 to 1000 μm which is availably gained by precision grinding. More attempts have focused on the improvement in size effect [10], minimum chip thickness [11], micro-milling forces [12], and burr formation [13]. Rapid tool wear for WC and PCD micro-mills is another critical problem in micro-milling. Nakamoto et al. [14] demonstrated that flank wear and micro-chipping often occurred on the tip edge of PCD micro-mills. Coating was also applied for micro-mills to improve their physical/mechanical properties. Ucun et al. [15] found that the uncoated micro-mill was prone to edge chipping and corner wear, while the AlCrN-coated micro-mill was first abraded off followed by flank wear and fracture and eventually failed. More edge chipping was observed by Kiswanto et al. [16] using the coated micro-mill to machine aluminum alloy 1100, and more adhesion wear and abrasion wear dominated during micro-milling of aluminum alloy 7075 demonstrated by Kuram et al. [17]. However, micro-mill life reported in most of the current literatures looked shorter relative to macro-mill life. Few investigations concerned the tool life in micro-milling especially, and up to now, few works investigated the feasibility to manufacture the micro-mills using cermet and further studied their cutting reliability. In our previous works [18, 19], a $Ti(C_7N_3)$-based ceramic insert was developed and a very good tool life was exhibited in macro-machining, and furthermore, this material was developed as micro-mill for milling aluminum alloy 2024, thus very good machining results and longer tool life were obtained.

Based on our previous works, this study attempts to deeply investigate the micro-milling performance and micro-machined channel quality of our developed cermet micro-mill with a wide range of cutting parameters during micro-milling aluminum alloy 2024. The comparative analysis of surface roughness and dimensional accuracy of channel, defect formation, tool life and chips were discussed. The feasibility of micro-mill manufactured by ceramic was verified and the optimum process of micro-milling aluminum alloy 2024 channel was given. Our work will lay foundation on developed new micro-tool with the aim of improving the micro-machining efficiency and understanding the failure mechanism of the new tool.

2 Experimental setup

The experiments have been performed by micro-milling channel on a hard aluminum alloy 2024 workpiece, which is used in aviation and aerospace industries because of its low density and excellent strength. Figure 1 shows the photo and SEM micrograph of cermet micro-mill that includes three main parts, namely the shank park, the neck part, and the cutting part. The diameters of shank part and cutting part are about 3 mm and 990 μm, respectively. This cermet micro-mill has two flutes with a helix angle of 15° and its edge radius ranges from 3 to 5 μm. The rake angle and flank range of micro-mill are set as 5° and 12°, respectively. The micro-milling experiments, as shown in Table 1, were designed to investigate the cermet micro-mill life and micro-milled channel quality. To eliminate the possible effects of workpiece micro-inclination due to the clamp on the ultra-precision five-axis micro-machining center (Nanotech 350FG, England), the surface on each workpiece was machined to flatness using a 6-mm tungsten carbide mill before experiments. Then, channels were machined using our developed cermet micro-mills. The micro-milled channels quality and tool wear were observed every 10 min using a laser scanning microscope (LSM, VKX200K; Keyence, Japan) and scanning electron microscopy (SEM; SUPRA55, Germany). The machine quality of channels was evaluated considering the surface defects and dimensional accuracy. The tool performance and chip morphology were also discussed in detail.

3 Results and discussions

3.1 Channel quality

3.1.1 Burrs

LSM and SEM micrographs of channels, micro-milled by a spindle of 30,000 r/min, feed of 1.0 μm/z, and depth of cut of 100 μm after 10 and 40 min, are shown in Fig. 2. Since some hard phases existing in the hard alumina alloy were removed forcedly during micro-milling, cavities were formed on the channel base. No obvious burrs were found on all channel

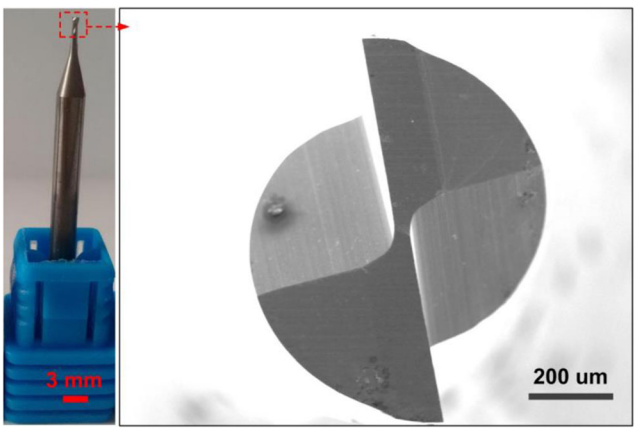

Fig. 1 Photo and SEM micrograph of cermet micro-mills

Table 1 The cutting parameters of micro-milling tests

Spindle speed (r/min)	Cutting speed (m/min)	Depth of cut (μm)	Feed (μm/z)
30,000	94	100	0.5
30,000	94	100	1
30,000	94	100	1.5
30,000	94	100	2
30,000	94	120	2
30,000	94	150	2
20,000	63	100	2
10,000	31	100	2

bases. The feed of 1.0 μm/z can be inclined to produce the top burrs of channel wall. An amount of top burrs have overgrown on the channel wall like full of brambles, and this problem became more serious as the milling time went on. On the basis of relations between tool rotation and feed direction, the left and right sides of the channel wall were machined by down-milling and up-milling, respectively. Burrs of down-milling side were characterized of tearing, fragmenting, and strips, while the whole flanging burrs appeared on the top of up-milling side. Furthermore, the down-milling brought about some bulges on the channel wall, which produced toward the channel; on the contrary, the up-milling generated some dimples on the channel wall. It is evident that both bulges and dimples can debase the dimensional accuracy of micro-milled channel. Figure 3 shows the 3D micrographs of micro-milled channel using a spindle speed of 30,000 r/min, feed of 2.0 μm/z, and depth of cut of 100 μm. The clearer cutting traces were always present on the surface of channel base compared with that milled at the lower feed (1.0 μm/z). After milling of 10 min, a channel with higher quality was gained because its base surface was very smooth and not any clearly visible top burrs were formed on the wall. Although some cavities were found on the base, it is related with some hard phases existing in the workpiece and independent of the cutting performance of cermet micro-mills. After milling of 40 min, some top burrs were caused on the channel wall and some plastic deformation also took place on the channel base, implying that tool wear weakened the sharpness of cutting edges and did not remove the workpiece materials effectively. However, top burrs at this cutting parameter were inferior to that at the lower feed, indicating that it was an appropriate method to optimize the machining processing strategies to minimize the burr formation.

Figure 4 shows the SEM micrographs and milled channels when the spindle speed was reduced and the depth of cut was increased. After machining of 10 min, a small fin rather than scrap burrs emerged on the top of channel wall at the low spindle speed, and a few small burrs had been initiated at the higher depth of cut. After 40 min, this fin had developed into burrs in Fig. 4b, and burrs and bulges in Fig. 4d had been as serious as those in Fig. 2c, indicating that the reduction of spindle speed alleviated the burr formation while the improvement of depth of cut promoted the burr formation. Although burr formation was retarded at the lower spindle speed, another matter (fins) was produced on the top of channel wall, which also influenced the machining quality and dimensional

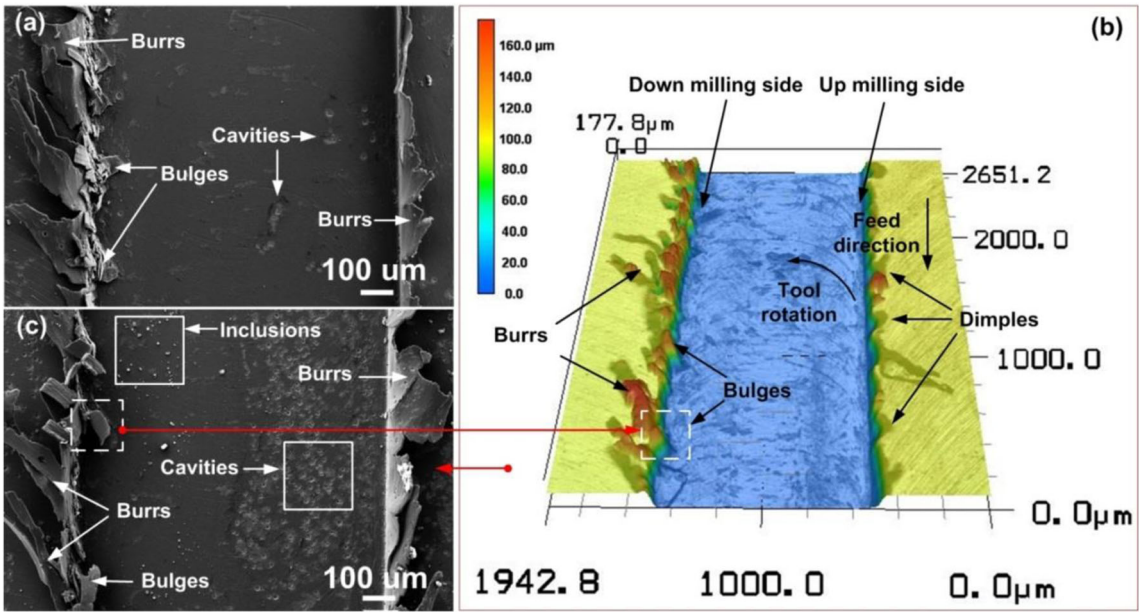

Fig. 2 LSM and SEM micrographs of channel micro-milled by a spindle speed of 30,000 r/min, feed of 1.0 μm/z, and depth of cut of 100 μm after 10 min (**a**) and 40 min (**b**, **c**)

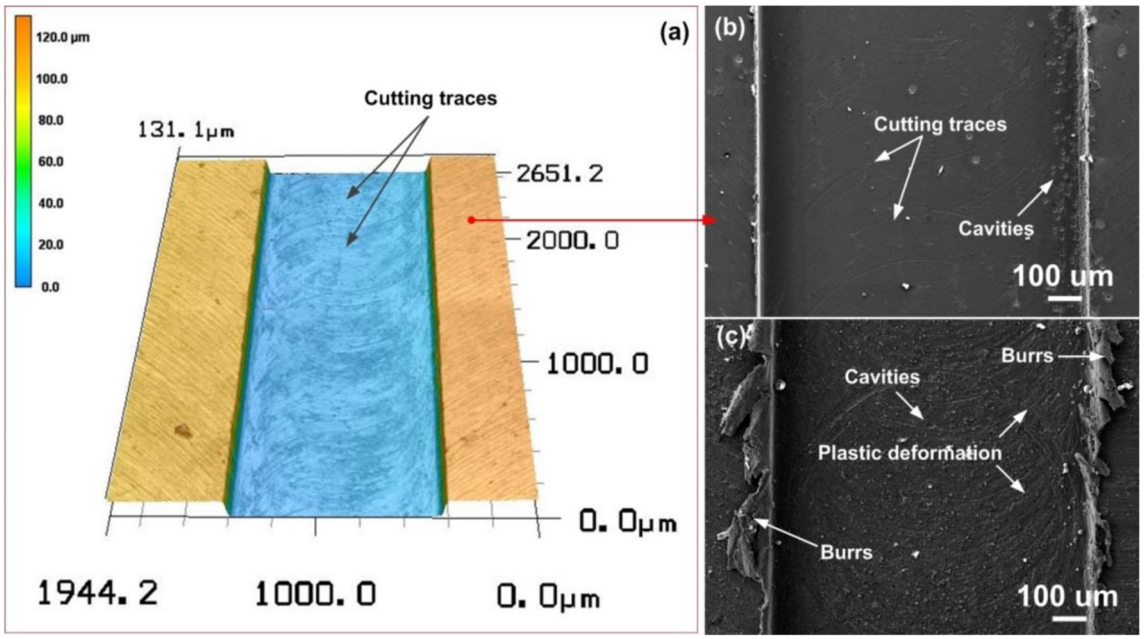

Fig. 3 LSM and SEM micrographs of channel micro-milled by a spindle speed of 30,000 r/min, feed of 2.0 μm/z, and depth of cut of 100 μm after 10 min (**a**, **b**) and 40 min (**c**)

accuracy of the channel. According to observations of different machining conditions, machined channels affected by burrs can be classified into three types given in Fig. 5. Figure 5a shows the best quality without few burrs. The two other channels of Fig. 5b and c were undesirable since an amount of burrs were generated on the top of channel wall, which is considered to be the most difficult to remove. Furthermore, these two channels had a different characteristic

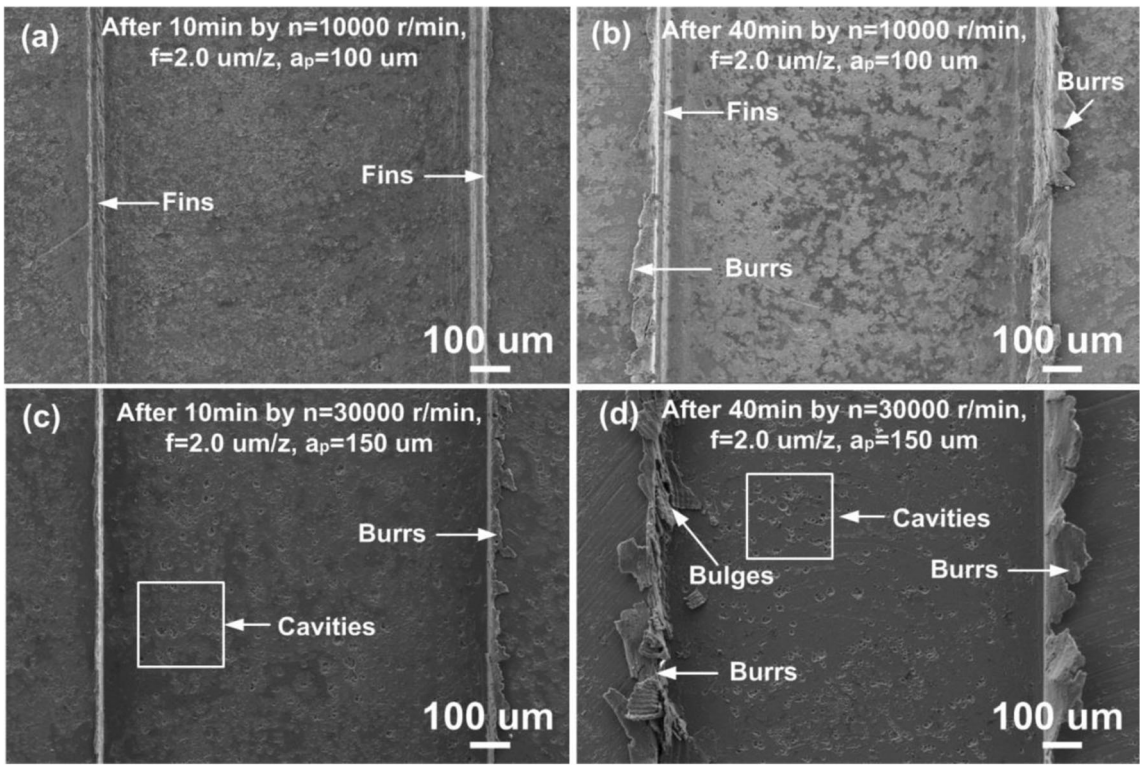

Fig. 4 SEM micrographs of micro-milled channels varying the spindle speed and depth of cut after 10 and 40 min, respectively

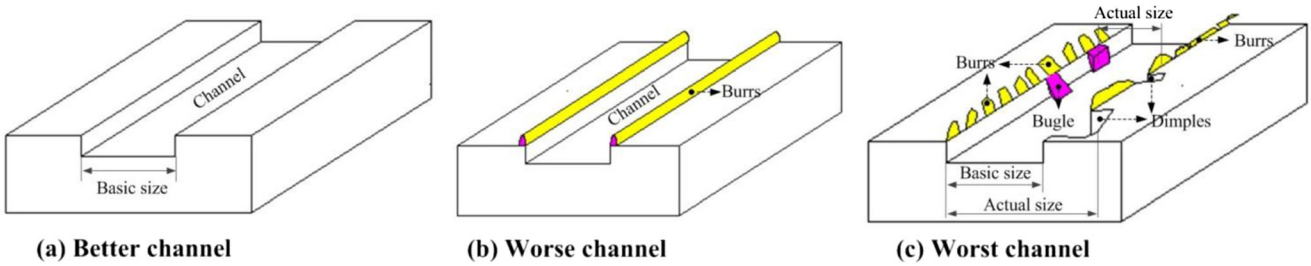

Fig. 5 Types of channels machined by cermet micro-mills

relating to the machining process. Burrs in Fig. 5b were more similar to fins flanging on the top of channel, which was characterized by a whole small piece. Burrs in Fig. 5c were visibly larger and wavier more like rags. This kind of burrs was also varied by milling methods. Since this machining belongs to slot milling, two sides of the channel experienced the up-milling and down-milling, respectively, responsible for the different shapes of burrs. Besides burrs, dimples and bulges were also found on up-milling and down-milling sides, respectively. Burrs are negative to channel quality in terms of deburring time and cost because removing of burrs from micro-parts is a tough task. Dimples and bulges induced a change of the local channel dimension to affect the assembly and serve performance of components. Bulges were to stick to the channel wall and protrude into the aisle, which could make the channel width size to decrease. Dimples were pits inside the channel wall, caused by tearing of burrs to form the wall, which caused the channel width size to increase. The dimensions of channel with the machining time were measured statistically to compile a tolerance zone diagram given in Fig. 6, where the basic size of channel is approximately equal to the tool diameter.

3.1.2 Dimensional accuracy of channel

Since the depth-to-width ratio of channel can reach 1:10, it is difficult to directly evaluate the surface quality of channel wall in accordance with the traditional standard of surface roughness. Moreover, the dimensional accuracy at the width direction is more important than that at the depth direction. Because the channel depth is far less than its width, any variation in the channel width is a key index in terms of both the dimensional accuracy and surface quality of micro-milled channel. The precision of micro-milled channel can be assessed by describing these tolerance zone diagrams. It is also used as a means of assessing the micro-machinability of cermet micro-mills because tool diameter directly determined the micro-milled channel width. The basic size of channel width is considered as 0.96 mm, which is slightly smaller than the initial diameter of micro-cutter because of elastic recovery of channel, and has to vary as tool wear processed with increasing cut time. Six 2.5-mm-long channels were collected to measure their width, separately, at the six time periods from 1 to 50 min in the micro-milling, as shown in Fig. 6. The minimal variation of channel dimension was seen at 94 m/min (30,000 r/min) cutting speed, 2 μm/z feed and 100 μm depth of cut, where the tolerance zone size of channel width was only 0.01 mm after milling of 20 min, and it slowly expanded to 0.03 mm after 50 min. The effects of feed, cutting speed, and depth of cut on the precision of channels are different. Feed and depth of cut had the more distinct influences on the channel widths. The feed of 1 μm/z or depth of cut of 150 μm resulted in bad channels like Fig. 5c, where the actual width size of micro-milled channel departed even further from the basic size. The actual width size smaller than the basic size should be relevant to three factors: elastic recovery of machined wall, uncut bulges adhering on the wall, and tool wear, whereas the larger actual width size than the basic size may be ascribed to the dimple generation in the wall. It is noted that the larger tolerance zone was not found for these cases of feed higher than 1.5 μm/z. In micro-milling process, relationships of feed with the cutting edge radius must be taken into consideration. No chips can be formed in every pass of the cutting edge below a critical threshold value called “minimum chip thickness” depending on the ratio of feed per tooth to radius of the cutting tool. It was hard for the 0.5 μm/z feed investigated in this study to impel chips to form, and for this case, the unremoved layer of worpiece material experienced squeezing, plowing, and elastic recovery as the micro-mills passed over the channel. This process of chip deformation did not bring about much variations of tolerance zone compared to the chip deformation for the 1.0 μm/z feed, where materials can be removed as a chip. Although the chip formation could cause the elastic deformation to decrease for this case, it made the tolerance zone of channel unstable. This means that the removing material encountered the transformation from plowing to cutting at the initial time of chip creation. The minimum chip thickness was dependent on the properties of the workpiece material, and for Al7075 material, it was found to be approximately 0.7 μm in the literature [20]. Our investigated hard aluminum alloy has a better ductile and certain hardness because of many phases in its microstructure, tending to form a chip by tearing material from the channel wall to produce many defects, such as dimples and bulges, depressing the dimensional accuracy.

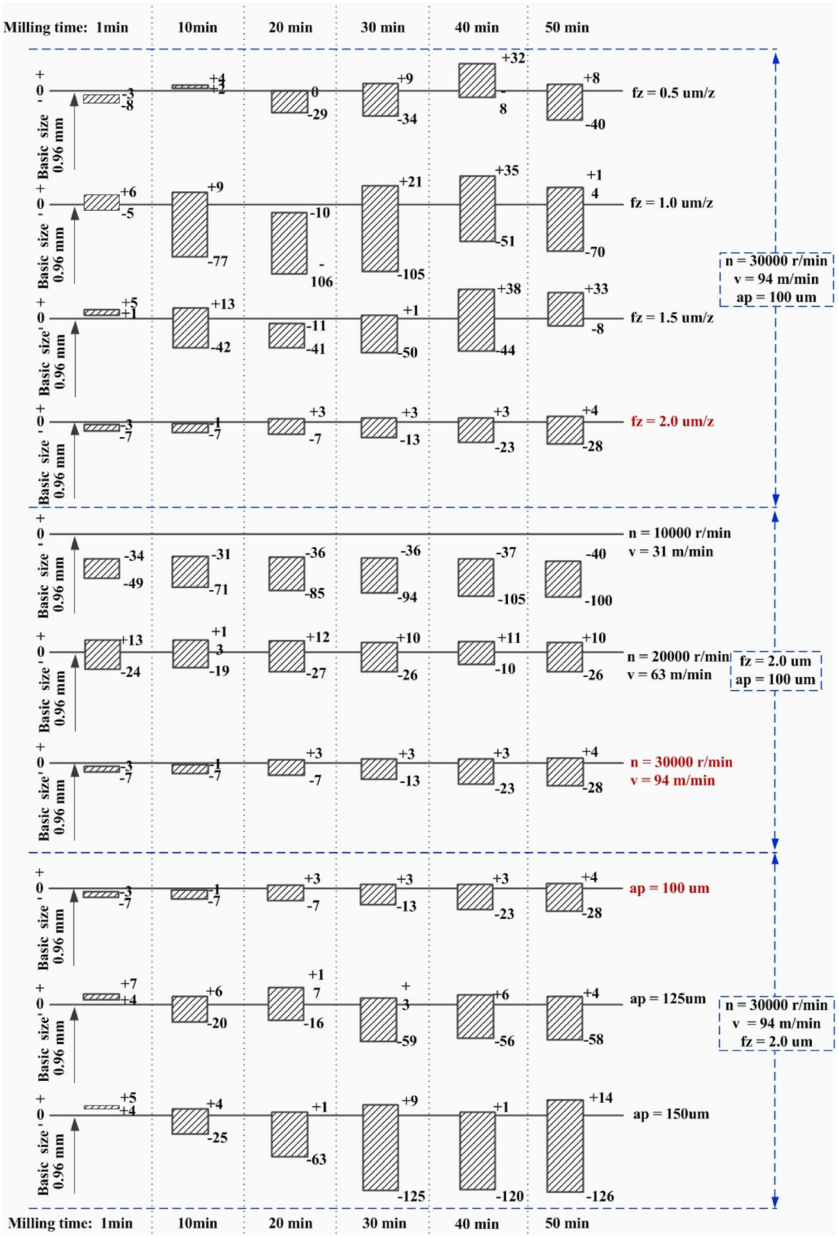

Fig. 6 Tolerance zone diagram of channels width under various cutting parameters in micro-milling

The reduction of channel dimension also resulted from the lower cutting speed. Specific energies are a measurer to evaluate the removal capacity to workpiece material, calculated by dividing the machining forces by the chip area. Filiz et al. [21] demonstrated that the specific energies increased with the increased speed because the effect of thermal softening of workpiece during micro-milling was less than the effect of the strain rate. It is apparent that the removal capacity of tool to workpiece was so insufficient at the lower cutting speed that a majority of the uncut materials elastically recovered after the tool passed. The elastic recovery of channel wall was associated with the reduction of the width dimension of channel.

The defect generation in milling process can be explained by the graphical description given in Fig. 7. The instantaneous chip area varies during a tool tooth pass, from zero at the beginning of engagement to the maximum value, and then back to zero at the exit of cut. When the feed rate is higher than the critical feed rate, the machining process can be illustrated in Machining Processing I. Supposing that edge A of tool first enters into cut and edge B is then engaged when edge A exits. The green and red crescents in Fig. 7a will be its corresponding nominal layer removed by edges A and B after rotating a circle. For the case of Machining Processing I (Fig. 7I(a)–(e)), when edge A passes over the channel, a chip

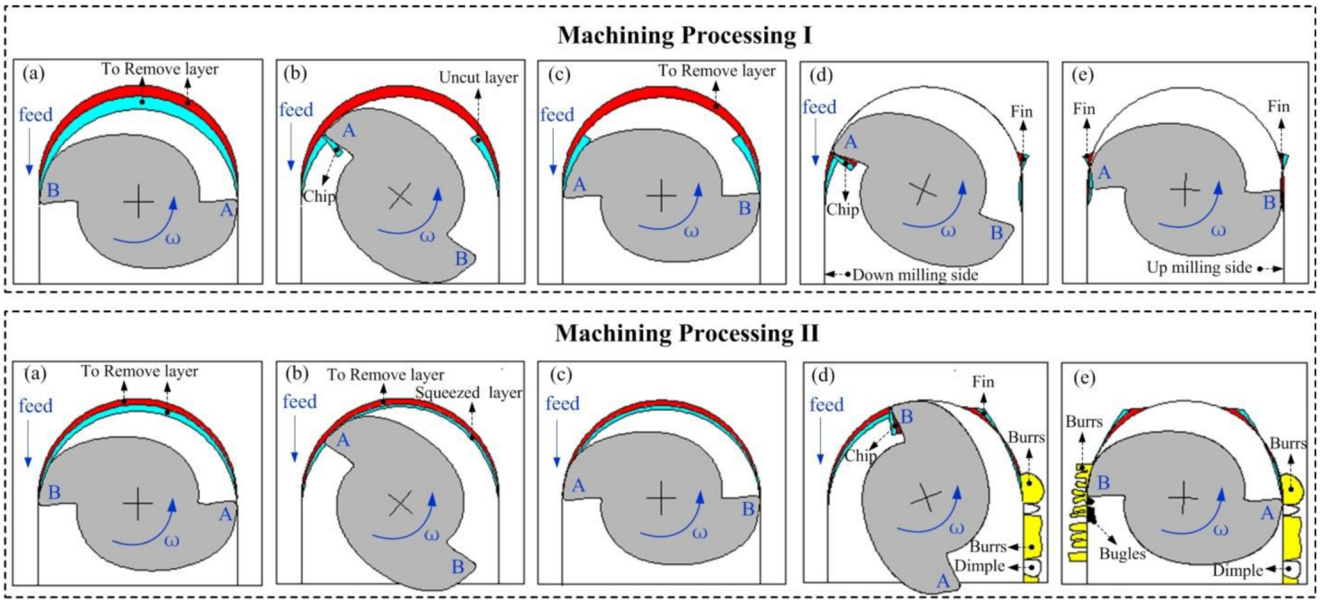

Fig. 7 Schematic illustration of surface defects formation and chip generation in micro-milling processing

can be created until the instantaneous chip thickness is larger than the critical thickness due to the cutting edge radius, and two uncut layers experience a squeezing action forced by the cutting tool land and still stay on the channel. When edge B passes again, the cutting regions of the removed layer has to be enlarged because the uncut layer left from the previous pass of edge A is accumulated to increase the instantaneous chip thickness. This also advances the initial point of chip creation at an earlier angular position, which diminishes the residual area of the uncut layer, forming the small burrs or fins. These demonstrate that the reasonable choice of the preferring machining process can control the formation of micro-milled surface defects. For the case of Machining Processing II (Fig. 7II(a)–(e)), because of the chip thickness smaller than the cutting edge radius, materials are not removed efficiently from the workpiece in the first pass of edge A. During this process, this process is involved with a very intense forcing action, including squeezing, shearing, and elastically recovering, and work hardening occurs successively (Fig. 7II(b)), and the majority of this material deformation has a negative effect on the following machining of edge B. In the following pas of edge B, a chip is not still generated if a critical threshold of chip creation is not reached despite the previous unremoved layer has been accumulated to this pass. However, the work hardening of residual material tends to enhance the difficulty in cutting for the following pass. Thus, edge B cannot cut the material down and this part of deformation material is not taken away and still remains along the channel top to be pushed outward by tool edge, then burrs are formed. Some materials also tear under large tensile stress from the top to form dimples. Bulges locating on the side of channel base occur because of the insufficient engagement with chips. However, bulges are more generated near the down-milling side of channel, and more burrs are generated near the up-milling side of channel. Li et al. [22] found that the up-milling produced the lower average force amplitude as compared to down-milling. Therefore, the higher cutting force caused more materials to be plowed rather than shear, tending to form these base dimples. These phenomena were more popular as the axial depth of cut or feed rate increased. The spindle speed also had an effect on the formation of surface defects in this work, but to a lesser degree than the feed and depth of cut. These surface defects were also affected strongly by tool wear, especially on the down-milling side. All of these surface defects deteriorated the machined quality and dimensional accuracy of channel.

3.1.3 Surface roughness of channel base

The machined quality channel can also be reflected by its base roughness. Despite cavities were distributed randomly because an amount of hard phases existed in the microstructure of the workpiece, the cutting parameters can still determine the surface roughness of channel base. The variations of base roughness with cutting parameters are shown in Fig. 8. The higher surface roughness of channel base was caused when the feed of 0.5 μm/z is used. At this case, the surface roughness rose rapidly to about 1.0 μm after cutting of 10 min, and produced a further increment after 50 min. The feed of 1.5 to 2.0 μm/z led to a good surface quality, and importantly, the surface roughness did not have an obvious change from the beginning machining to 50 min in the micro-milling. The cutting edge of micro-mills could not remove the workpiece material efficiently at the lower feed. In this condition, the sharp cutting edge was worn for a few minutes because of the intensive plowing of tool on aluminum, and the cutting

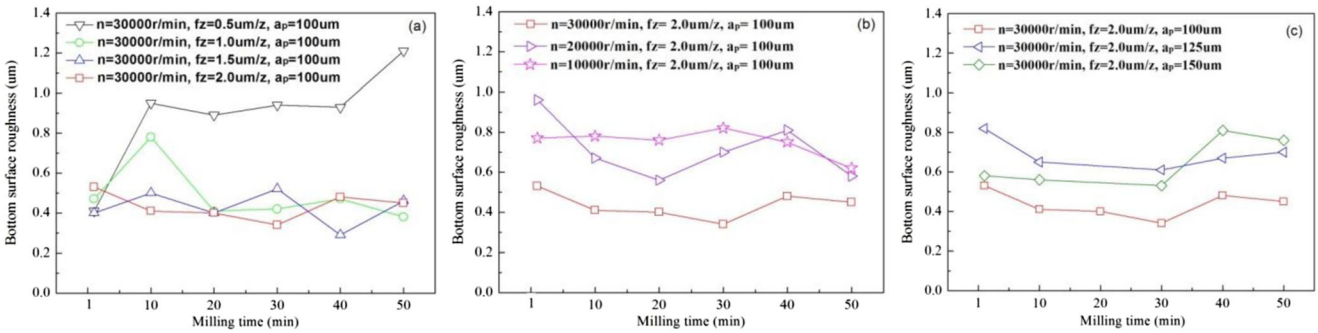

Fig. 8 Effects of cutting parameters on surface roughness of channel base

of 50 min had caused the cutting edge to fail. However, tools still kept some degree of sharpness at the feed of 1.5–2.0 μm according to variations of surface roughness during micro-milling. Though there are not many differences between surface roughness caused by depths of cut of 125 and 150 μm, the increase of depth of cut reduced the surface quality of channel base. In these cases, as the machining progressed, some great changes took place in the surface roughness at the different milling stages. Importantly, the higher surface roughness values were found after the milling time is more than 30 min. The decreased cutting speed evidently caused the increased surface roughness. For the high-strength material such as hard aluminum alloys 2024, some hard-brittle phases were dislodged leaving the cavities, accompanied by the removing of chip. Unlike channel wall, few obvious burrs were found on the channel base, which indicates that effects of burrs on base roughness are negligible. In terms of lower feed, higher depth of cut, and longer milling time, massive cavities appeared on the channel base as shown in Figs. 1, 2, 3, and 4, thus determining the bad surface quality. The undesired surface quality and increased surface roughness tended to result from the cutting parameters of 10,000–20,000 r/min spindle speed, 0.5–1.0 μm/z feed, and 125–150 mm depth of cut. Therefore, the preferred cutting parameters should avoid this range.

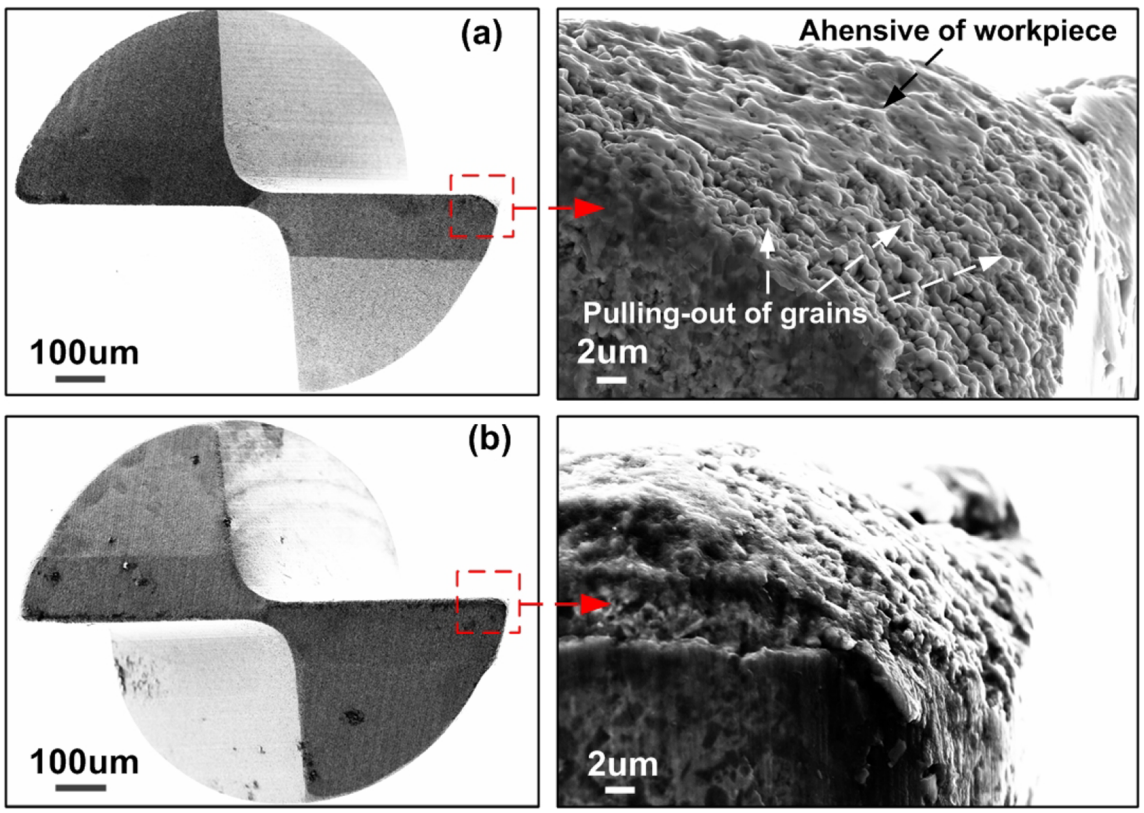

Fig. 9 SEM micrographs of tool wear at spindle speed of 30,000 r/min and depth of cut of 100 μm for different feeds: 0.5 μm/z (**a**, **b**) and 2.0 μm (**c**, **d**), reported in our previous work (Xu and Zou 2016)

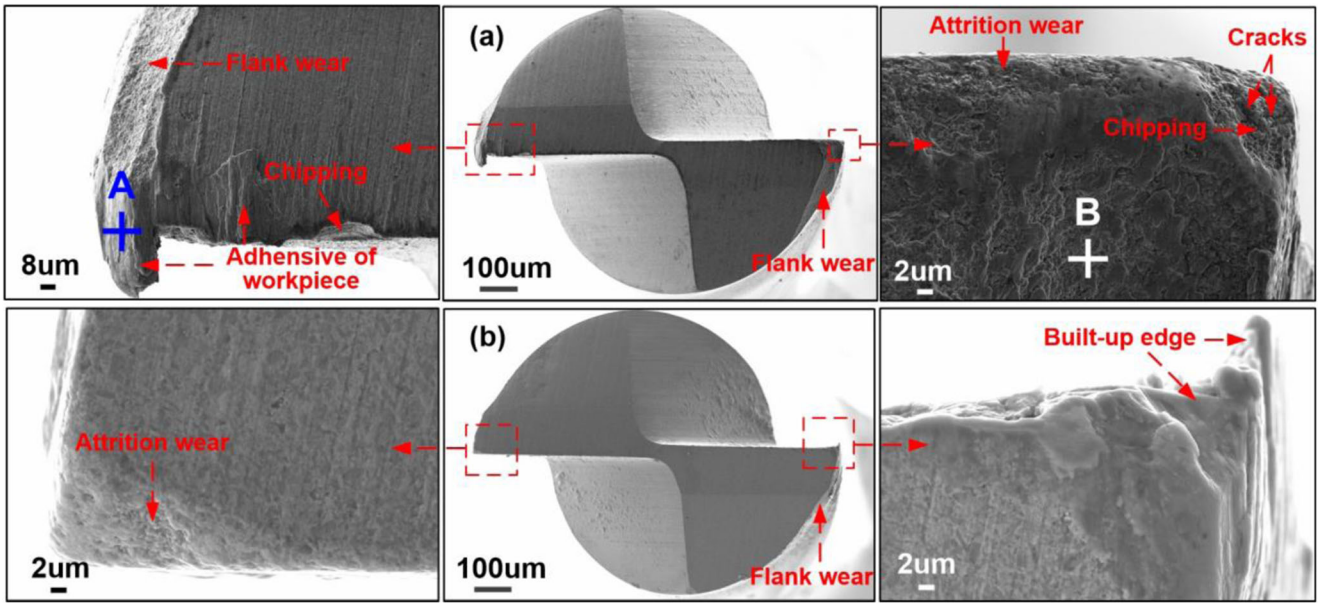

Fig. 10 SEM micrographs of tool wear at **a** spindle speed of 10,000 r/min, feed of 2.0 μm/z, and depth of cut of 100 μm; and **b** spindle speed of 30,000 r/min, feed of 2.0 μm/z, and depth of cut of 150 μm

3.2 Tool life

Our previous work [19] have testified that our developed cermet micro-mills have a better tool performance than WC micro-mills in micro-milling aluminum alloy due to a sharper tool tip can be gained on cermet micro-mills. SEM micrographs of worn tool at different cutting parameters after machining 50 min are given in Figs. 9 and 10. Though micro-cracks and fracture were encountered at tool tip and flank, no tool breakage was present for cermet micro-mills. The tool tip was abraded at 30,000 r/min spindle speed and 100 μm depth of cut for any of feed (see Fig. 9). The aluminum alloy 2024 is a soft material but has an excellent strength, which can induce a stress high enough to wipe off tool tip during micro-milling. This process also caused individual Ti(CN) grains to dislodge from metal binders of tool, and then some workpiece materials build-up filled the cavities formed by these pulling-out of Ti(CN) grains. More cavities remained after more grains dislodged on the worn tool tip at the low feed, where the higher indentation/plowing actions forced by micro-milling induced the higher stresses to individual Ti(CN) grains. However, this wear mode of tool tip belonged to attrition wear. The attrition wear rate of tool tip is higher for 0.5 μm/z feed than 2.0 μm/z feed, comparing Fig. 9a to b. The severe tool wear occurred when the spindle speed decreased or the depth of cut increased, as shown in Fig. 10. For the case of low spindle speed, more wear modes such as cracks, chipping, adhesion, and desquamation emerged beside tool tip wear. The worn flank region mainly located at the junction of the major flank and minor flank, where some tool materials were desquamated from the tool body. It is well known that tools at low cutting speed are in the cut for longer periods of time, which forced the flank to encounter a longer shearing and friction action with the elastically recovered machined surface. Figure 6 also indicates that the channel diameter

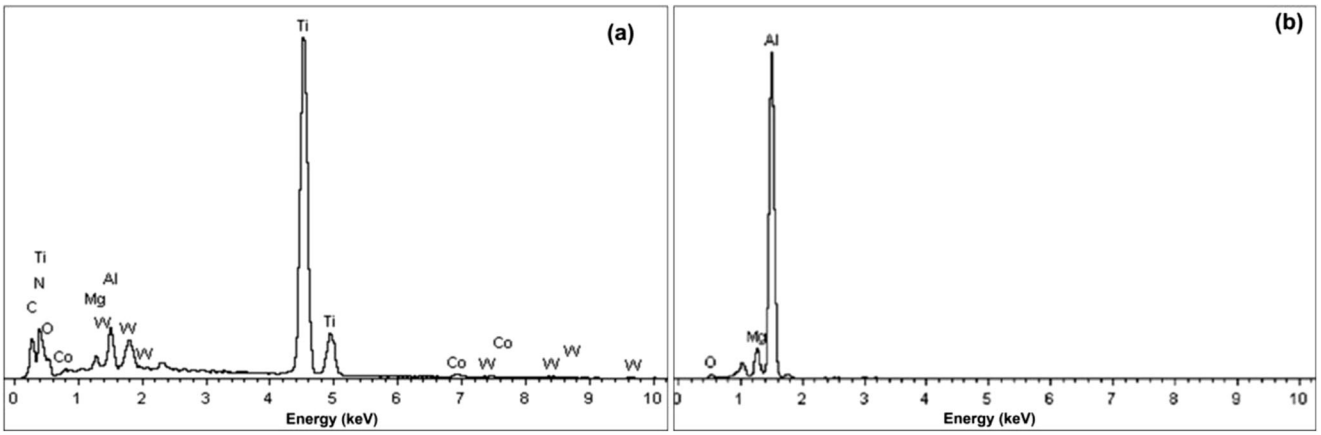

Fig. 11 EDS patterns of worn tool corresponding to points A and B in Fig. 10

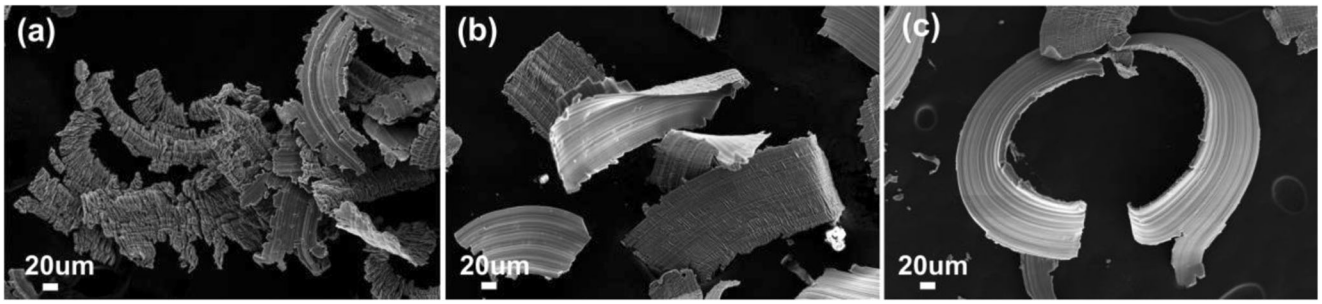

Fig. 12 Chip morphology under various feed rates: **a** 0.5 μm/z, **b** 1 μm/z, and **c** 2 μm/z, reported in our previous work (Xu and Zou 2016)

was reduced significantly with the machining time. Since the widths of the micro-milled channels could be used as a measure of tool wear progression [21], the severe flank wear of micro-mills caused to the reduction of tool diameter, then was responsible for the reduction of channel diameter. The EDS analysis in Fig. 11 also revealed that a stack of workpiece material deposited on the exposed micro-tool tip comprised mainly Mg and Al, indicating the occurrence of adhesive wear. Despite the very small removal volume for micro-milling aluminum alloy 2024, the removal materials underwent a violent gradient change of stress and strain which may release a higher heat in a small region between cutting edge and chips, and these machining heats could diffuse out through the close contact between the tool–chip and tool–workpiece. This process was obviously restricted from the limited chip extraction due to the low cutting speed. However, these adhesives on the tool tip were prone to fall off during machining, and took some tool material away from tool tip, which were demonstrated by the present cracks at the position of tip chipping in Fig. 10a. The flank wear also weakened the stiffness of tool tip to accelerate the tool failure. Since the dull tool tip increased the cutting force, it is anticipated that tool wear occurred more rapidly and machined channel quality deteriorated at the lower spindle speed. For the case of high depth of cut, severe flank wear also found (Fig. 10b), whereas some workpiece materials were caught by tool tip as built-up edge. The built-up edge replaced the tool tip to machine in favor of protecting the tool tip and resisting micro-tool wear. On the contrary, once the built-up edge was broken away from tool tip, the machining vibration was activated and the tool diameter was reduced to worsen the machined channel quality.

3.3 Chips

The chip and its types are very important to evaluate the machined surface quality and tool life in micro-machining [23, 24]. Figures 12 and 13 show the chip morphology at various cutting parameters. At 0.5 μm/z feed rate, the produced chips exhibited a crushed state, indicating that the undeformed chip thickness was less thick than the minimum chip thickness and the dominant chip formation was the indentation/plowing in its most basic form (Fig. 12a), where this process was similar to grinding. A standard C-shape chip was generated at 2.0 μm/z feed (Fig. 12c) as the minimum chip thickness and plowing effects were reduced, and the majority of this process was controlled by shearing. When the spindle speed was decreased to 10,000 r/min, many long continuous chips were formed (Fig. 13a), indicating that the reduction of micro-milling speed depressed the work hardening and coefficient of deformation of chip, leading to the long continuous chip not to facilitate to be broken. When the depth of cut was increased to 150 μm at 30,000 r/min spindle speed and 2.0 μm/z feed, the broken-shape chip appeared, like these chips generated by 30,000 r/min spindle speed, 1.0 μm/z feed, and 100 μm depth of cut. Since tool wear was serious and the channel quality was poor, this shape of chips was undesirable at these cutting parameters. The smaller chip size means more materials were removed and affected by the plowing effect during micro-milling [25], which was one of the primary reasons that these cutting parameters tended to create the larger burrs.

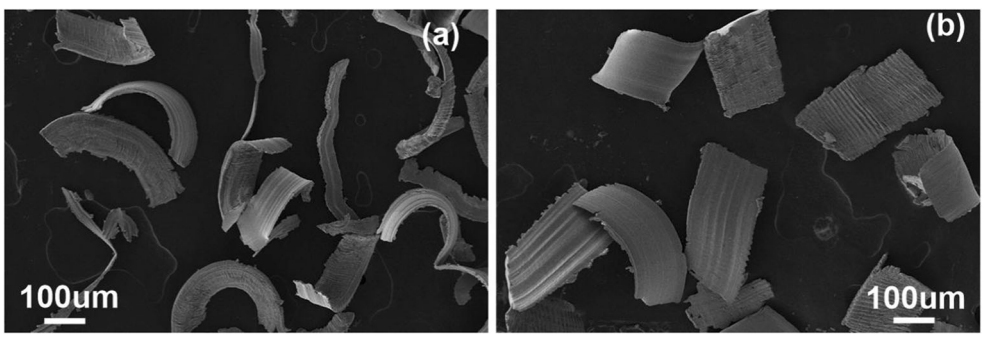

Fig. 13 Chip morphology at **a** spindle speed of 10,000 r/min, feed of 2.0 μm/z, and depth of cut of 100 μm; and **b** spindle speed of 30,000 r/min, feed of 2.0 μm/z, and depth of cut of 150 μm

4 Conclusions

Cermet micro-mill is a new developed cutting tool and its tool performance and cutting capacity were rarely reported. The following specific conclusions have been drawn from this investigation:

1. The spindle speed of 30,000 r/min, feed of 2.0 μm/z, and depth of cut of 100 μm is suitable for our developed cermet micro-mill to machine the channel of aluminum alloy. The edge radium of cermet micro-mills can be smaller than 5 μm, having two flutes with a helix angle of 15°. The cermet micro-mills exhibited a very good tool performance in terms of a good quality and high accuracy of channel with few small burrs, and longer tool life. This was ascribed to the sharpness of tool tips and its maintenance due to higher hardness of cermet.
2. Burrs tended to appear on the top of channel wall for the cases of lower spindle, lower feed, and higher depth of cut. The down-milling and up-milling were responsible for different qualities of micro-milled channel wall. The down-milling produced burrs characterized by tearing, fragmenting, and strips, and further created some bulges on the channel wall. The up-milling brought about flanging burrs, which further tended to generate some dimples on the channel wall. However, both bulges and dimples can debase the dimensional accuracy of micro-milled channel. The 1.0 μm/z feed or 150 μm depth of cut led the dimensional accuracy to depart even further from the basic size due to formation of many bulges and dimples. The 10,000 r/min spindle speed facilitated to reduce the channel width because of the elastic recovery of channel wall after a tool pass.
3. No obvious burrs were found on all channel bases. The surface roughness of channel base was dependent of cavities, which is controlled by the cutting conditions. At the cutting parameters of 10,000–20,000 r/min spindle speed, 0.5–1.0 μm/z feed, and 125–150 mm depth of cut, massive cavities appeared on the channel base to deteriorate the surface quality. The lower feed rate also was prone to the higher surface roughness because of intensive plowing of tool on aluminum caused by the rapid tool wear.
4. No tool breakage was present for cermet micro-mills. Tool wear was dominated by attrition wear at the optimum cutting condition. Besides tip wear, failure modes such as cracks, chipping, adhesion, and desquamation occurred at the other cutting conditions. The severe flank wear appeared at the low cutting speed or higher depth of cut, which weakened the stiffness of tool tip to accelerate the tool failure. A standard C-shape chip was generated at 2.0 μm/z and the majority of this process was controlled by shearing.

Acknowledgments This project was supported by Shandong Science Fund for Distinguished Young Scholars (JQ201715) and the National Natural Science Foundation of China (no. 51575322).

References

1. Davim JP (2014) Modern mechanical engineering. Springer, London
2. Gupta MC, Li B, Gadag S, Chou KC (2010) Laser micromachining for fatigue and fracture mechanics applications. Opt Lasers Eng 48: 441–447
3. Jan AC, Reichenbach IG, Schuler GM (2012) Manufacture and application of ultra-small micro end mills. CIRP Ann-Manuf Technol 61:83–86
4. Zhan ZB, He N, Li L, Shrestha R, Liu JY, Wang SL (2015) Precision milling of tungsten carbide with micro PCD milling tool. Int J Adv Manuf Technol 77:2095–2103
5. Suzuki H, Okada M, Fujii K, Matsui S, Yamagata Y (2013) Development of micro milling tool made of single crystalline diamond for ceramic cutting. CIRP Ann Manuf Technol 62:59–62
6. Cheng X, Wang ZG, Nakamoto K, Yamazaki K (2010) Design and development of PCD micro straight edge end mills for micro/nano machining of hard and brittle materials. J Mech Sci Tech 24:2261–2268
7. Cheng X, Wang Z, Nakamoto K, Yamazaki K (2011) A study on the micro tooling for micro/nano milling. Int J Adv Manuf Technol 53:523–533
8. Egashira K, Hosono S, Takemoto S, Masao Y (2011) Fabrication and cutting performance of cemented tungsten carbide microcutting tools. Precis Eng 35:547–553
9. Aurich JC, Reichenbach IG, Schüler GM (2012) Manufacture and application of ultra-small micro end mills. CIRP Ann-Manuf Technol 61:83–86
10. Cuba AR, Autenrieth H, Strau T, Deuchert M, Hoffmeister J (2012) Characterization of the transition from ploughing to cutting in micro machining and evaluation of the minimum itchiness of cut. J Mater Process Technol 212:594–600
11. Fernanado DO, Alessandro RR, Reginaldo TC, Adriano FS (2015) Size effect and minimum chip thickness in micromilling. Int J Mach Tools Manuf 89:39–54
12. Annoni M, Biella G, Rebaioli L, Semeraro Q (2013) Microcutting force prediction by means of a slip-line field force model. Procedia CIRP 8:558–563
13. Mamedov A, Lazoglu I (2016) An evaluation of micro milling chip thickness models for the process mechanics. Int J Adv Manuf Technol 87:1843–1849
14. Nakamoto K, Katahira K, Ohmori H, Yamazaki K, Aoyama TY (2012) A study on the quality of micro-machined surfaces on tungsten carbide generated by PCD micro end-milling. CIRP Ann-Manuf Technol 61:567–570
15. Ucun I, Aslantas K, Bedir F (2013) An experimental investigation of the effect coating material on tool wear in micro milling of Inconel 718 super alloy. Wear 300:8–19
16. Kiswanto G, Zariatin DL, Ko TJ (2014) The effect of spindle speed, feed-rate and machining time to the surface roughness and burr formation of aluminium alloy 1100 in micro-milling operation. J Manuf Process 16:435–450
17. Kuram E, Ozcelik B (2013) Multi-objective optimization using Taguchi based grey relational analysis for micro-milling of Al 7075 material with ball nose end mill. Measurement 46:1849–1864

18. Zou B, Zhou HJ, Xu KT, Huang CZ, Wang J, Li SS (2014) Study of a hot-pressed sintering preparation of Ti(C_7N_3)-based composite cermets materials and their performance as cutting tools. J Alloy Compd 611:363–371
19. Xu KT, Zou B, Wang YS, Guo P, Huang CZ, Wang J (2016) An experimental investigation of micro-machinability of aluminium alloy 2024 using Ti(C_7N_3)-based cermet micro end-mill tools. J Mater Process Technol 235:13–17
20. Park SS, Malekian M (2009) Mechanistic modeling and accurate measurement of micro end milling forces. CIRP Ann-Manuf Technol 58:49–52
21. Filiz S, Conley MC, Wasserman MB, Ozdoganlar OB (2007) An experimental investigation of micro-machinability of copper 101 using tungsten carbide micro-endmills. Int J Mach Tools Manuf 47:1008–1100
22. Li P, Zdebski D, Langen HH, Hoogstrate AM (2011) Micromilling of thin ribs with high aspect ratios. J Micromech Microeng 20:13–23
23. Mamedov A, Lazoglu I (2016) An evaluation of micro milling chip thickness models for the process mechanics. Int J Adv Manuf Technol 87:1843–1849
24. Rezaei H, Sadeghi MH, Budak E (2018) Determination of minimum uncut chip thickness under various machining conditions during micro-milling of Ti-6Al-4V. Int J Adv Manuf Technol 95:1617–1634
25. Sooraj V, Mathew J (2011) An experimental investigation on the machining characteristics of microscale end milling. Int J Adv Manu Technol 56:951–958